Time-Reversal Through-Wall Microwave Imaging in Rich Scattering Environment Based on Target Initial Reflection Method

Amin B. Gorji and Bijan Zakeri

Department of Electrical and Computer Engineering
Babol Noshirvani University of Technology, Babol, Iran
amin.gorji@stu.nit.ac.ir, zakeri@nit.ac.ir

Abstract ─ In recent years, time reversal (TR) methods have been widely employed in microwave imaging (MI) applications due to their efficient functionality in heterogeneous media. One of the applications turning into a great interest is through-wall microwave imaging (TWMI). In this paper, classic TR method is applied to detect and localize a target obscured by a brick wall inside a rich scattering environment using numerically generated data. Regarding this, it is shown when the signals acquired by a set of receivers are time reversed and backpropagated to the background media, finding an optimum time frame which the constituted image represents a true location of the target becomes infeasible. Indeed, based on target distance and increasing multiple scattering in the media the previously-used maximum E-field method and entropy-based methods fail to select the optimum time frame. As a result, an improved procedure named target initial reflection method (TIRM) is proposed. Even in the case of rich scattering environment, the results show this method prevails over the incapabilities of the former methods.

Index Terms ─ Finite-difference time-domain (FDTD), optimum focusing, rich scattering environment, target initial reflection method (TIRM), through-wall microwave imaging, time reversal (TR).

I. INTRODUCTION

In the area of microwave imaging (MI), the great interest on detection and localization of objects through walls and obstacles has been emerging in recent years. This phenomenon basically arises from various unique civilian and military applications, including non-destructive evaluations, earthquake search and rescue missions, hostage operations or hostile threat assessment situations [1]. In fact, a through-wall microwave imaging (TWMI) system would be capable of collecting information of the total media consisting of target(s) and wall(s), performing a comprehensive process on it, and then identify and localize the target. The way of how to process the collected data in order to get the best performance of the system has opened a gate to the advent and development of various techniques in the last decade. Encouraging results have been obtained with backscattering algorithms [2], synthetic-aperture-radar (SAR) [3], polarimetric-based techniques [4], tomographic approach [5], and high-speed imaging algorithm known as Envelope [6].

However, among the processing algorithms, time reversal (TR) methods have shown that would exploit ultrawideband (UWB) signals and the concept of multipath components in the intervening media to ameliorate the detection capabilities [7]. Originally, TR has been utilized in acoustics [8], but later on has been introduced in electromagnetics and more research has been carried out on subsurface object imaging [9], wireless communication systems [10], bio-malignant tissue detection in early stage breast cancer [11]-[13], and most recently through-wall imaging of the obscured targets [14]-[17].

In TR method, a source radiates a signal to be propagated through a media including the target. The waves are then reflected and the corresponding data are recorded by an array of receivers. By extracting the target responses from the data, reversing them in time and synthetically propagating them back from their respective reception points, an image of the scene is constituted at each time frame, consequently by utilizing an appropriate approach to take an optimum time frame, detection and localization of the target becomes possible. Furthermore, in TWMI applications, TR entails to detect targets through materials including plywood, drywall, solid/hollow brick and concrete, which their relative high permittivity or inhomogeneous structure may result in further burden for selecting the optimum time frame.

In this paper, we embark on solving the problem of finding an optimum time frame which represents a true image of the target. In this regard, maximum electric-field (E-field) method [14] and entropy-based methods [11], [12], [15], [16] have been recently employed in both TWMI and breast cancer detection scenarios. These methods may guarantee maximum amplitude or a tightly focused image corresponding to the detected location of

Submitted On: January 1, 2014
Accepted On: May 10, 2015

the target. However, we show there are situations based on target distance and rich scattering environment in which the preceding methods fail to image the true location of the target. As a result, an alternative improved method, based on initial reflection from the target, which is robust to the effect of these parameters and prevails over previous methods is proposed.

The rest of the paper is organized as follows: in Section II a general description and fundamental theories of TR method for inverse scattering problem is presented. In Section III, the geometry of TWMI problems along with the specifications of computational setup which is carried out numerically using finite-difference time-domain (FDTD) [18] is introduced. In Section IV, the methods of finding an optimum time frame together with the proposed method are fully addressed. The results regarding the performance of the methods to successfully localize the target are completely demonstrated in Sections V. Finally, in Section VI, a summary of the present work and the future contributions is drawn.

II. TR METHOD

A. TR overview

Time reversal (TR) technique is an imaging method based on the invariance of Maxwell's equations under time reversal, which in electromagnetics is known as the principle of reciprocity. In general, the procedure for detection and localization of the scatterer (target) based on TR consists of three main steps shown in Fig. 1.

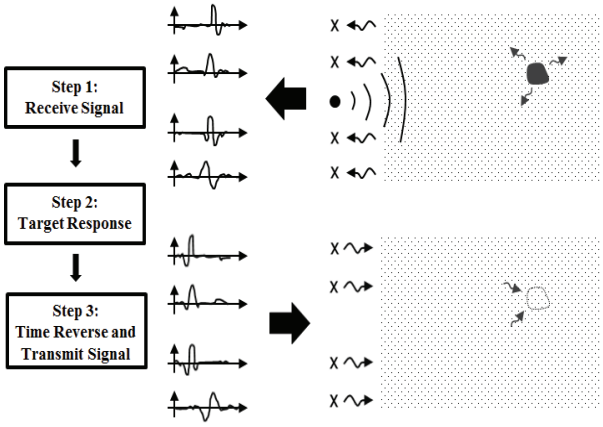

Fig. 1. General scheme of TR method. A source radiates a signal and the scatterer reflects a portion of it back to the TRA. The target responses are then reversed in time and backpropagated to the background media, eventually space-time focusing is achieved at the target location.

First, a source radiates a signal to be propagated through an arbitrary media including the targets as well. Then, the reflected fields from the media are recorded by an array of receiving antennas which in an ideal situation, should be placed all around the media to capture all the possible directions of the reflected waves. However, unlike this full-aspect configuration [19], in other types of scenarios, it is presumably impossible to entirely surround the media and a limited number of arrays are particularly feasible. This limited-aspect configuration is in prevalent use for the applications including TWMI and subsurface objects imaging. Thereupon, the aim of forward propagation step is to collect the data of the media and process them in order to image and localize the targets. Accordingly, the data can be generated either analytically [7], [20], numerically [11]-[14], or physically via on-site measurement [21], in which the first two suffices when one deals with the development of imaging algorithms in the way that spending time and energy on practical measurements is almost cumbersome.

Next, the target response must be extracted from the recorded signal at each array receiver. Since the recorded signal of the media consists of background clutter plus target, assuming that the background is stationary, its solo signature with no target in present can be calculated and collected at each receiver. Now let's assign E_T and E_B as the total and background reflected signals, respectively. Then for each receiver, the target (scattered) response E_S is obtained as:

$$E_S = E_T - E_B . \tag{1}$$

This method of extracting the target response is called background subtraction method. In fact, extracting the target response is the basis of all TR processing methods including Classic TR [11], [12], DORT [9], [22], MUSIC [23] and TRAIC [24]. In scenarios in which E_B cannot be obtained separately, the target response is directly extracted from the total response by applying a time-window on the total signal [9] or matched-filter analysis [25]. However, these methods will surely yield more mathematical efforts. Additionally, in moving target scenarios, the information about E_B may not be required and corresponding target response can be achieved using the total response subtraction of two successive moving target runs. This method is called differential TR and is fully addressed in [26].

In the final step, based on TR processing method used in the previous step, imaging and localization of the target become possible. By time-reversing (phase conjugating in frequency domain) the target responses at each array receiver and synthetically propagating them back to the background media (no target), the wave focuses on the location of target, approximately recreating an image of it. It is obvious this step is performed computationally either analytically by using Green functionals named point spread functions (PSF) [27] or numerically including FDTD [11]-[14], TLM [28], and Ray-Tracing methods [29]. Despite this, unlike the imaging applications, physical back propagation of

the waves may be applied in applications involving actual retransmission of signals such as destruction of kidney stones with ultrasonic waves [30].

B. TR theory of inverse scattering problem

General fundamental theories of TR method can be addressed as following. Suppose a source located at r_s which emits a time domain pulse $P(t)$, and an array of K receivers each located at r_k as in Fig. 2. The fields incident on the target area at r' is then given by:

$$\begin{aligned} E_F(r',t) &= P(t) * G_F(r_s, r', t) \\ &= \int P(\tau) G_F(r_s, r', t-\tau) d\tau \ , \end{aligned} \tag{2}$$

where $G_F(r_s,r,t)$ is the Green's function between any representative point in the media (background+traget) and the radiating point in forward-propagation step. Noting that physical interaction of antennas are not considered and the asterisks * represents time-domain convolution. Here, for the sake of conciseness we are considering scalar two-dimensional form of the fields and Green's functions. Extension to the vector case is also straightforward in principle, but may be complicated to be expressed in general form.

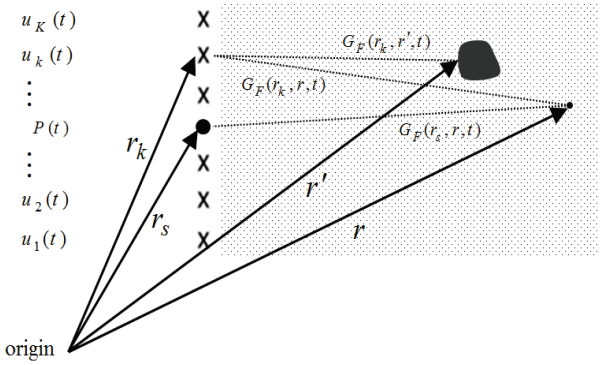

(a)

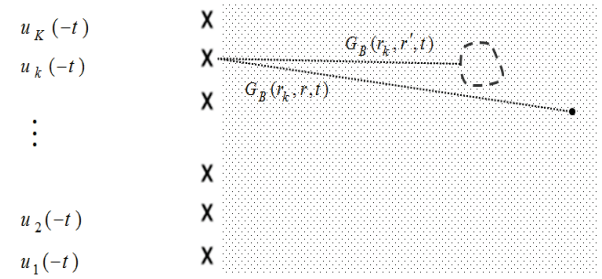

(b)

Fig. 2. TR theory of inverse scattering problem. The source is placed at the center of TRA and the corresponding Green's function between TRA and any point in the media is specified: (a) forward-propagation, and (b) back-propagation.

In continue, the fields are scattered by the target, ignoring multiple interactions between the target and the background media, which is analogous to first order scattering model (Born approximation) [31], the field observed at k^{th} receiver is then obtained as in equation (3). Considering the higher orders of scattering models including second order model and full multiple scattering interactions using Foldy-Lax equations are also investigated in [32]:

$$u_k(t) = \int_{\text{on target}} B(r') E(r',t) * G_F(r', r_k, t) ds' \ , \tag{3}$$

where $B(r')$ is the scattering coefficient of each point on the target area. In fact $B(r')$ represents the conversion of incident fields $E(r',t)$ into equivalent currents that re-radiate as the secondary sources.

Reducing the integral in equation (3) using a high-frequency asymptotic approximation, which is a case for well-resolved point like scatterer, $u_k(t)$ is simplified to:

$$u_k(t) = \hat{B}(r') P(t) * G_F(r_s, r', t) * G_F(r', r_k, t) \ . \tag{4}$$

It is notable that $\hat{B}(r')$ accounts for all terms introduced by the asymptotic approximation, and thus, can be inferred as the average scattering coefficient of the target.

To perform TR process, the scattered fields recorded at each array are time-reversed and back-propagated from their respective positions. The field observed at each point r in the imaging domain is obtained by:

$$E_B(r,t) = \sum_{k=1}^{K} u_k(-t) * G_B(r_k, r, t) \ , \tag{5}$$

where $G_B(r_k,r,t)$ is the Green's function between any representative point in the background-only media and the k^{th} receiver in back-propagation step. Equation (5) is solely enough for one to perform an imaging and localization process using the collected raw data of $u_k(t)$ (actually without knowing about the terms appeared in (4)), and a precise estimation of G_B. The way to estimate G_B, either analytically or numerically is the main core of TR method, particularly for the scenarios in which no exact knowledge about the background media is available [16].

Now, we proceed our discussion to analytically investigate and show how a constructive interference will happen in the imaging domain where $E_B(r,t)$ will respond to the target location. Let's expand equation (5) using equation (4) to obtain equation (6) as:

$$\begin{aligned} E_B(r,t) &= \sum_{k=1}^{K} u_k(-t) * G_B(r_k, r, t) \\ &= \sum_{k=1}^{K} \hat{B}(r') P(-t) * G_F(r_s, r', -t) \\ &\quad * G_F(r', r_k, -t) * G_B(r_k, r, t) \ , \end{aligned} \tag{6}$$

because of reciprocity,

$$G_F(r,r_k,t)=G_F(r_k,r,t). \quad (7)$$

According to Fig. 2, it is interpreted that the only point in which $G_F(r_k,r,t)$ is equivalent to $G_B(r_k,r,t)$ is the location of the formerly existing target, which means for $r=r'$. So,

$$G_F(r_k,r',t)=G_B(r_k,r',t). \quad (8)$$

Using equations (7)-(8) and rewriting equation (6) for $r=r'$, $E_B(r',t)$ is obtained as:

$$E_B(r',t)=\sum_{k=1}^{K}\hat{B}(r')P(-t)*G_F(r_s,r',-t) *G_B(r_k,r',-t)*G_B(r_k,r',t). \quad (9)$$

Based on equation (9), $G_B(r_k,r',-t)*G_B(r_k,r',t)$ is indeed representing a matched-filter with a maximum at $t=0$. As a result, maximum of $E_B(r,t)$ happens for spatial-temporal location of $r=r'$ and $t=0$ (optimum time frame) which in fact the location of the target.

Further discussion about the interpretation of $t=0$ is given in section IV, where we are dealing in more details with the optimum time methods to focus the waves on the true location of the target.

III. GEOMETRY AND COMPUTATIONAL SETUP

A. Geometry of rich scattering environment

The geometries of rich scattering environment for TWMI problem considered in this work are shown in Fig 3. A standard commercial solid brick cell with ε_r=4.8 and σ=0.001 S/m [33] is used to construct a wall with 10 cm thickness at the front and inner partitions with 5 cm thickness behind it. A linear array with aperture size of a=90 cm consisting of 16 isolated z-directed infinitesimal electric dipoles with equidistant separation of 6 cm are placed 20 cm in front of the wall to act as the receiving probes. These probes are also in use as the transmitter in synthetically backpropagation step of TR imaging algorithm. A z-directed electric dipole is also placed at the center of the array line as the monostatic transceiver to cylindrically radiate the excitation signal toward the scene in TM_z mode. More information regarding TE_z and full polarimetric polarization can also be found in [34]. A cylindrical disk scatterer with diameter D=6 cm and distance L away from the array with ε_r=47 is introduced as the target in near distance for L/a<1 (Fig. 3 (a)) and far distance for L/a>1 (Fig. 3 (b)). The locations of the target are shown in Table 1.

Table 1: Target locations for TWMI problem

Target Location (x,y)	(70,40)	(160,85)
Distance Ratio L/a	(near) < 1	(far) > 1

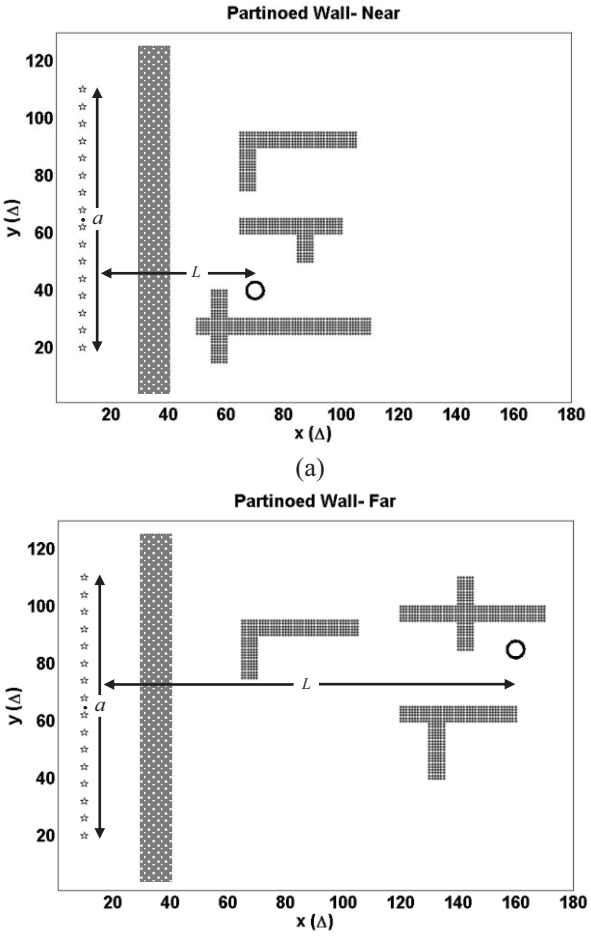

Fig. 3. Geometry of rich scattering environment for TWMI problem. The source (dot) and TRA (stars) are shown. The aperture size and target distance are also denoted by a and L, respectively. The target is located at: (a) near distance, and (b) far distance.

B. FDTD computational setup

Both forward-propagation and back-propagation steps of TR method are carried out numerically using two-dimensional finite-difference-time-domain (FDTD) method. Taking into account the standard FDTD notation, the update equations of back-propagation step for TM_z case take the following form as in equations (10)-(12).

$$H_x^{n'+\frac{1}{2}}(i,j+\tfrac{1}{2})=\left(\frac{1-\frac{\sigma(i,j)\Delta t}{2\mu(i,j)}}{1+\frac{\sigma(i,j)\Delta t}{2\mu(i,j)}}\right)H_x^{n'-\frac{1}{2}}(i,j+\tfrac{1}{2})+ \left(\frac{\frac{\Delta t}{\mu(i,j)}}{1+\frac{\sigma(i,j)\Delta t}{2\mu(i,j)}}\right)\left(-\frac{E_z^{n'}(i,j+1)-E_z^{n'}(i,j)}{\Delta y}\right), \quad (10)$$

$$H_y^{n'+\frac{1}{2}}(\mathrm{i}+\tfrac{1}{2},\mathrm{j}) = \left(\frac{1-\frac{\sigma(\mathrm{i},\mathrm{j})\Delta t}{2\mu(\mathrm{i},\mathrm{j})}}{1+\frac{\sigma(\mathrm{i},\mathrm{j})\Delta t}{2\mu(\mathrm{i},\mathrm{j})}}\right) H_y^{n'-\frac{1}{2}}(\mathrm{i}+\tfrac{1}{2},\mathrm{j}) + \left(\frac{\frac{\Delta t}{\mu(\mathrm{i},\mathrm{j})}}{1+\frac{\sigma(\mathrm{i},\mathrm{j})\Delta t}{2\mu(\mathrm{i},\mathrm{j})}}\right)\left(\frac{E_z^{n'}(\mathrm{i}+1,\mathrm{j}) - E_z^{n'}(\mathrm{i},\mathrm{j})}{\Delta x}\right), \quad (11)$$

$$E_z^{n'+1}(\mathrm{i},\mathrm{j}) = \left(\frac{1-\frac{\sigma(\mathrm{i},\mathrm{j})\Delta t}{2\varepsilon(\mathrm{i},\mathrm{j})}}{1+\frac{\sigma(\mathrm{i},\mathrm{j})\Delta t}{2\varepsilon(\mathrm{i},\mathrm{j})}}\right) E_z^{n'}(\mathrm{i},\mathrm{j}) + \left(\frac{\frac{\Delta t}{\varepsilon(\mathrm{i},\mathrm{j})}}{1+\frac{\sigma(\mathrm{i},\mathrm{j})\Delta t}{2\varepsilon(\mathrm{i},\mathrm{j})}}\right)\left(\frac{H_y^{n'+\frac{1}{2}}(\mathrm{i}+\frac{1}{2},\mathrm{j}) - H_y^{n'+\frac{1}{2}}(\mathrm{i}-\frac{1}{2},\mathrm{j})}{\Delta x} - \frac{H_x^{n'+\frac{1}{2}}(\mathrm{i},\mathrm{j}+\frac{1}{2}) - H_x^{n'+\frac{1}{2}}(\mathrm{i},\mathrm{j}-\frac{1}{2})}{\Delta y}\right), \quad (12)$$

where n′ is the time step corresponding to backpropagation step. The 2D computational domain is gridded into dimensions of X×Y=180×130 cm, with a uniform spatial discretization of Δx=Δy=Δs and a time step of Δt (the stability Courant Factor S_c=c*Δt/Δs is chosen to be 0.5). The value of Δs is so assigned to create at least 10 nodes per λ_m, where λ_m denotes the wavelength corresponding to the maximum frequency content of the excitation signal. The maximum runtime is also set to maxtime=600Δt for near distance target and maxtime=1200Δt for far distance target which are sufficiently enough for the incident wave to travel from the source to the right end of the domain in a round-trip. The boundary condition is also a convolutional perfectly matched layer (CPML) formulated with recursive-convolution technique to provide reflectionless truncation of the computation domain. The thickness of CPML is set to 5Δs at all four sides of the boundaries.

It is also worth noting that in medium with high losses or dispersion, the performance of TR imaging based on standard FDTD may become degraded due to double attenuation in forward and back propagation steps. To dispel this problem, a modification on FDTD update equations may be performed at back-propagation step in order to compensate for losses or dispersion caused by the background media [11], [35].

C. Excitation signal

In general, various constraints and specifications including particular electrical characteristics of the media, signal penetration through wall materials, target dimensions, and also portability of the setup will determine the best operating frequency range for microwave penetrating radar (MPR) systems. Practically such systems operate in the range of 0.5-10 GHz [36] and a minimum system bandwidth of nearly to 30% with respect to the center frequency is essential for providing sufficient resolution for target detection [4]. In this work, a UWB Modulated Gaussian pulse is considered as the excitation sources by:

$$P(t) = e^{\left(\frac{t-t_s}{t_p}\right)^2}.\sin\left(2\pi f_p(t-t_s)\right), \quad (13)$$

where t_p and t_s are temporal width and temporal shift, respectively, which specify the spectrum bandwidth of $P(t)$ and f_p is the center frequency. These parameters are then assigned as f_p=1.95 GHz, t_p=0.35 ns and t_s=2*t_p which stimulate the target in Mie (resonance) scattering mode [37]. The excitation pulse and its frequency spectrum are also depicted in Fig. 4.

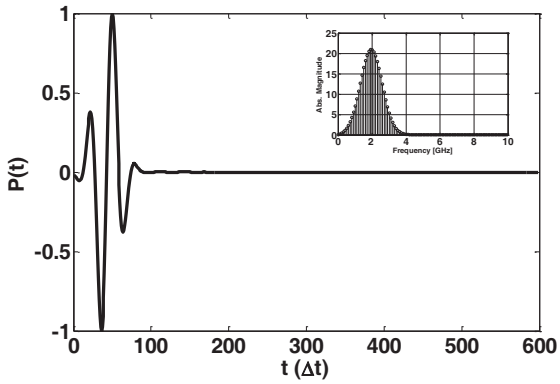

Fig. 4. Modulated Gaussian excitation signal source and its frequency spectrum for f_p = 1.95 GHz, t_p = 0.35 ns, and t_s = 2*t_p.

IV. OPTIMUM TIME FRAME METHODS

After exciting the source and collecting the data of the reflected signals, we obtain target responses by using background subtraction methods. The target responses are then time reversed and backpropagated to the background media consisting of the front wall and inner partitions with no prior information of the target location. Accordingly, the computationally backpropagated fields constitute an image of the scene at each frame of the time. Next, we embark on solving a problem of finding an optimum time frame which represents an image of the scene with true focusing on target location.

A. Maximum E-field method

As reported by Zheng, et al. [14], in this method the maximum electric field amplitude of the imaging domain at each time frame is found and then plotted along the time axis. The optimum time frame is then selected as a time which corresponds to the maximum of this plot, as:

$$t_{opt}^{\text{Zheng}} = \left\{t' : E_{\max}(t') > E_{\max}(t),\ t_0 < t < t_1 \ \ \&\ \ t \neq t'\right\}. \quad (14)$$

B. Entropy-based methods

In an ideal full-aspect configuration, the behavior of backpropagated waves on target location is such that it first converges toward the target and a time after that it diverges from it. In order to find a time frame which is

corresponding to the convergence-divergence instant, a minimum entropy criterion will be defined as in (16) and (17) reported by Cresp, et al. [15] and Kosmas, et al. [11], respectively:

$$p_{ij}^{n} = \frac{E_n{}^2(i,j)}{\sum\sum_{i,j} E_n{}^2(i,j)}, \tag{15}$$

$$\overset{\text{Cresp}}{ENT}(n) = \frac{-\sum\sum p_{ij}^{n} \ln p_{ij}^{n}}{\max(p_{ij}^{n})}, \tag{16}$$

$$\overset{\text{Kosmas}}{ENT}(n) = \frac{\left[\sum\sum_{i,j} E_n{}^2(i,j)\right]^2}{\sum\sum_{i,j} E_n{}^4(i,j)}, \tag{17}$$

where n represents the time frame, (i,j) the grid cell coordinates and the summation is over the entire imaging domain. The defined entropy is calculated at each time frame and a time instant when it becomes minimized is selected as an optimum time frame. Unlike the previous method, minimum entropy method guarantees a tightly focused image rather than maximum field amplitude at the focusing point.

C. Target initial reflection method (TIRM)

In this work, we examine the functionality and efficiency of the above focusing methods and investigate the situations in which they may fail to image the true location of the target. As a result, an alternative optimum time focusing method which is valid for all situations and prevails over the shortcomings of other methods must be utilized. In this part we are attempting to characterize this proposed method, named target initial reflection method (TI-RM), which is primarily based on ray-tracing method.

Let's postulate the geometry of a wall and a target which is placed in an arbitrary location in free space as shown in Fig. 5. Now, we follow the transmitted wave starting at the source point, propagating into the scene, possessing interactions with the wall and the target, and then reflecting back to the receiving arrays. In addition, we are interested to monitor the target response waveforms of three particular receivers; the source receiver, which corresponds to a receiver at the source point (R_S), the nearest receiver to the target (R_N), and the farthest receiver away from the target (R_F). The source is excited and after a delay of t_d it reaches to the corresponded peak value. In its path toward the target, it travels the route A_1B_1, B_1C_1 and C_1D, where D is the point which the transmitted wavefront is incident on the target. The target scatters the fields and a portion of them are received by the arrays. For the source receiver R_S, the scattered wave travels DC_1, C_1B_1 and B_1A_1, likewise the wave travels DC_2, C_2B_2 and B_2A_2 to reach to nearest receiver R_N, and DC_3, C_3B_3 and B_3A_3 to reach to farthest receiver R_F. The detailed waveforms monitored by each of these three receivers are shown in Fig. 6.

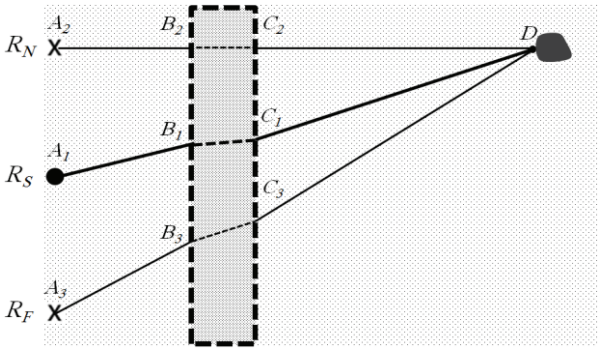

Fig. 5. Detailed route path of forward and back propagated waveforms for source receiver (R_S), nearest receiver (R_N), and farthest receiver (R_F).

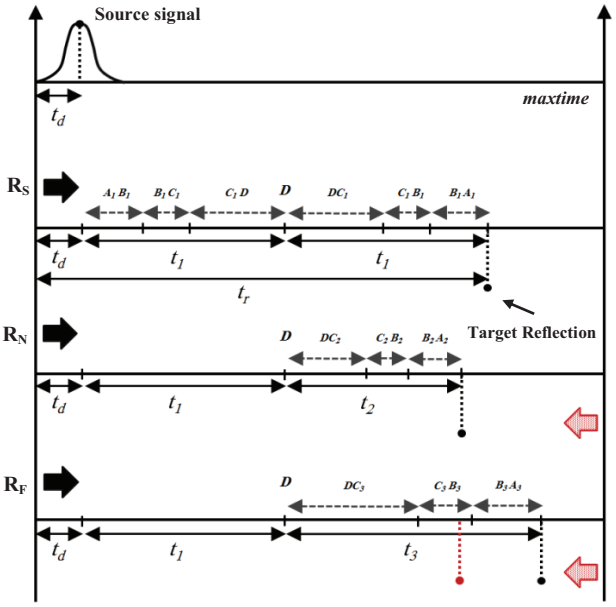

Fig. 6. Signal waveforms monitored by each of source receiver (R_S), nearest receiver (R_N), and farthest receiver (R_F). Time reversing and backpropagating the waveform is analogous to start propagation from the right end of the axis.

The received fields are then time-reversed and back-propagated, which is analogous to start the propagation from the right end of each waveform (maxtime) and move toward the left (Fig. 6). According to the depicted waveforms, the first antenna starting backpropagation process is the farthest one, it travels along the path toward the target up until the time the nearest antenna as the last antenna starts backpropagation. Based on Fig. 6, it is derived that the two waveforms will simultaneously

reach the target location D if they both travel only the remained time amount of t_2, which is the stacked time for the scattered waveform to travel from the target D to the nearest receiver at A_2. As a result, these two waveforms together with the waveform from the rest of the arrays will arrive at the same time to point D and their amplitudes are constructively added to each other to construct a contrasted image of the location of he target. More detailed route path of backpropagated waveforms are shown in Fig. 5.

In other words, the optimum time frame is a time instant in which the nearest receiver R_N is powered on and then continues traveling for t_2 sec. To formulize the optimum time, we may write:

$$t_{opt} = \underbrace{\left(\text{maxtime-}(t_d + t_1 + t_2)\right)}_{R_N \text{ is powered on}} + t_2 \qquad (18)$$

$$= \text{maxtime} - (t_d + t_1) \ ,$$

where t_1 is the stacked time for the source waveform to travel from starting point A_1 to target D or vice versa. According to the waveform of the source receiver,

$$t_r = t_d + 2t_1 \longrightarrow t_1 = \frac{t_r - t_d}{2}, \qquad (19)$$

where t_r is the time when the initial reflection from the target arrives to the source receiver. As a result by knowing the maxtime along with t_d and t_r, substituting equation (19) in equation (18), the optimum time frame t_{opt} could be readily derived as:

$$t_{opt} = \text{maxtime} - \frac{t_r + t_d}{2} \ . \qquad (20)$$

The optimum time frame based on TIRM guarantees well that the back-propagated waves of the entire receivers will simultaneously focus on a desired location which represents the target location. In the next section, it is investigated that this method yields to accurate results even in the case of rich scattering environment.

V. TARGET LOCALIZATION AND RESULTS

In this section, we are going through the localization of target for the geometries showed in Fig. 3 and apply focusing methods introduced in Section IV to select the optimum time frame for target location. Figure 7 shows the corresponding curves for each of focusing methods. Plots of Fig. 7 (a) and Fig. 7 (b) pertain to near and far distance ratios of the target, respectively. The optimum time frame derived by TIRM is determined by a vertical dashed line in each case. All the curves are plotted starting from 200Δt which is an instant the backpropagated waves pass the wall, up to the corresponding maximum runtime. The curves are also normalized with respect to their maximum value in order to become possible to be compared with each other. As it can be seen, in general plots of maximum E-field method have an increasing manner as it reaches to the maximum and then starts to descend. The entropy-based methods may also face inconsistent manner in the case of rich scattering environment rather than a monotonically decreasing manner, which is observed in the case of free space background [38]. Table 2 shows the optimum time frame concluded from the above curves for each method. The difference (in terms of Δt) between each method with respect to TIRM is also cited in the parentheses.

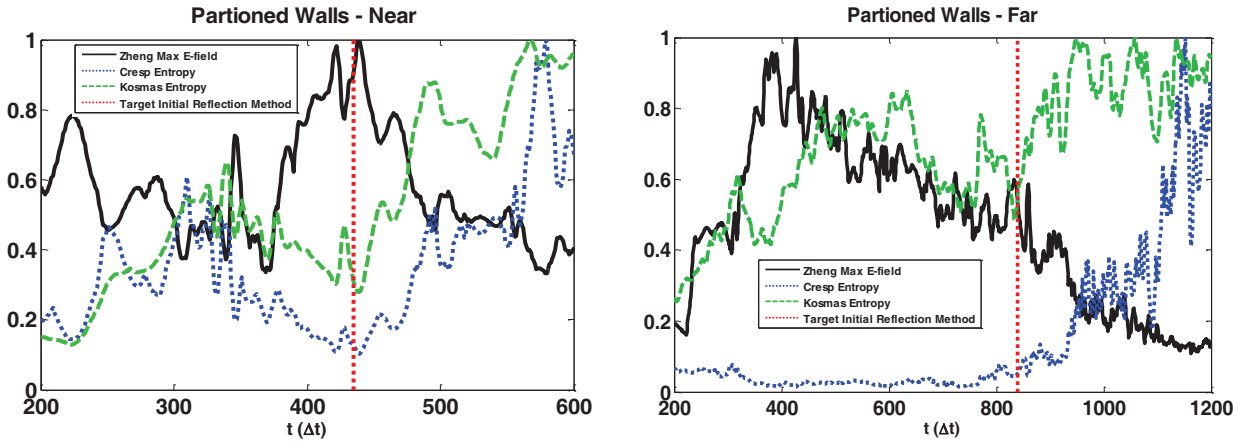

Fig. 7. Curves of optimum time frame for Zheng maximum E-field method, Cresp entropy-based method Eq. (16), Kosmas entropy-based method Eq. (17), and Target Initial Reflection Method (TIRM). (a) Near distance target, and (b) far distance target.

Table 2: Optimum time frame concluded from each method

	Near Distance	Far Distance
Zheng max E-field	439 (4)	427 (413)
Cresp entropy	439 (4)	733 (107)
Kosmas entropy	222 (213)	200 (640)
TIRM	435	840

Next, the images of spatial refocusing constituted by each method are demonstrated in Fig. 8 and Fig. 9 regarding near distance and far distance target location, respectively. The focused wave features a red spot and the true location of the target is drawn as a small circle. For near distance target (Fig. 8), it is clear from the images that the accurate focusing is almost achieved for all the methods including maximum E-field method, entropy-based methods, and TIRM. However entropy-based method of equation (17) yields an amount of displacement which is observed in the case of rich scattering environment. On the other hand, when target is located at far distance (Fig. 9), for all methods except TIRM, focusing is achieved with considerable amount of displacement to left from the true location of the target which leads to an inaccurate estimation about the existence of the target at its true location. It can be seen that no spot representing the target is even constituted for maximum E-field method and entropy-based method of equation (17).

More quantitative comparison of the images are depicted in Fig. 10, where for each method, the difference between the estimated location of the target and the true location is calculated and represented on account of target diameter D. In addition, the same results corresponded to free space case is also derived to further compare the effect of rich scattering environment on the performance of TR optimum time frame methods.

It is evident from Fig. 10, that when multiple scattering in the medium increases, for near distance target the performance of entropy-based method of equation (17) is degraded. All other methods including maximum E-field method, entropy-based method of equation (16), and TIRM are improved and they could estimate the target with less than 50 percent (0.5ΔD) displacement error. This improvement is in accordance with the concept of TR method that more scattering in the medium increases the spatial-temporal resolution of the focused waves. On the other hand, for far distance target the performance of all former optimum time frame methods are substantially degraded for both free space and rich scattering environment. However, the only method estimating the location of the target as accurate as possible is TIRM with still approximately less than 50 percent (0.5ΔD) displacement error which is quite appreciable. In general, we can conclude that TIRM prevails over all other methods without being totally dependent on the target near/far locations and free space or rich scattering background.

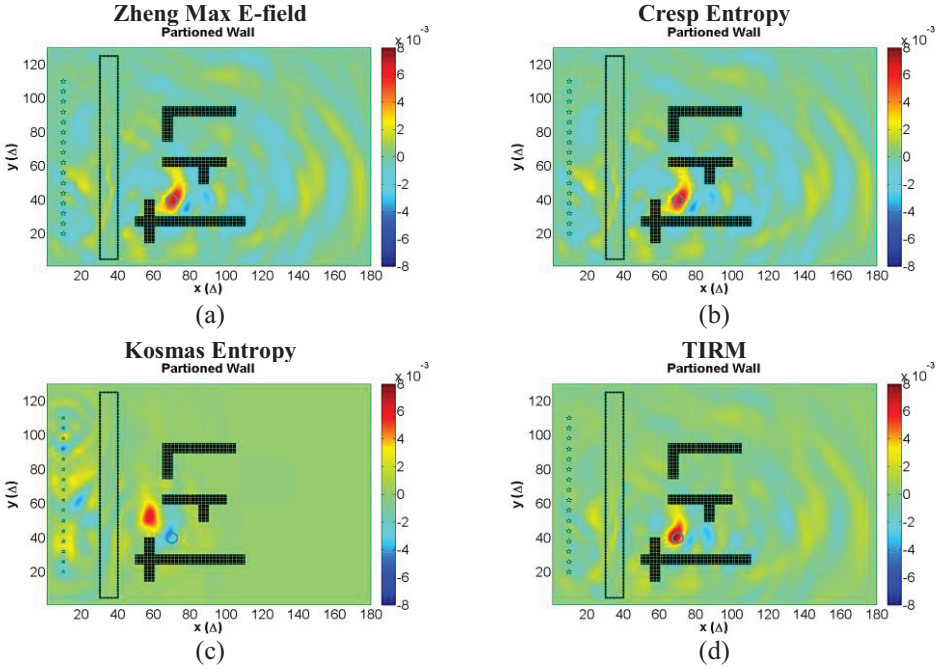

Fig. 8. The images constituted by TR method for target located at near distance. (a) Zheng Maximum E-field Method, (b) Cresp Entropy-based Methods Eq. (16), (c) Kosmas Entropy-based Methods Eq. (17), (d) TIRM. It is seen true focusing is achieved for almost of them. However, Kosmas Entropy-based method faces an amount of displacement to left with respect to the target.

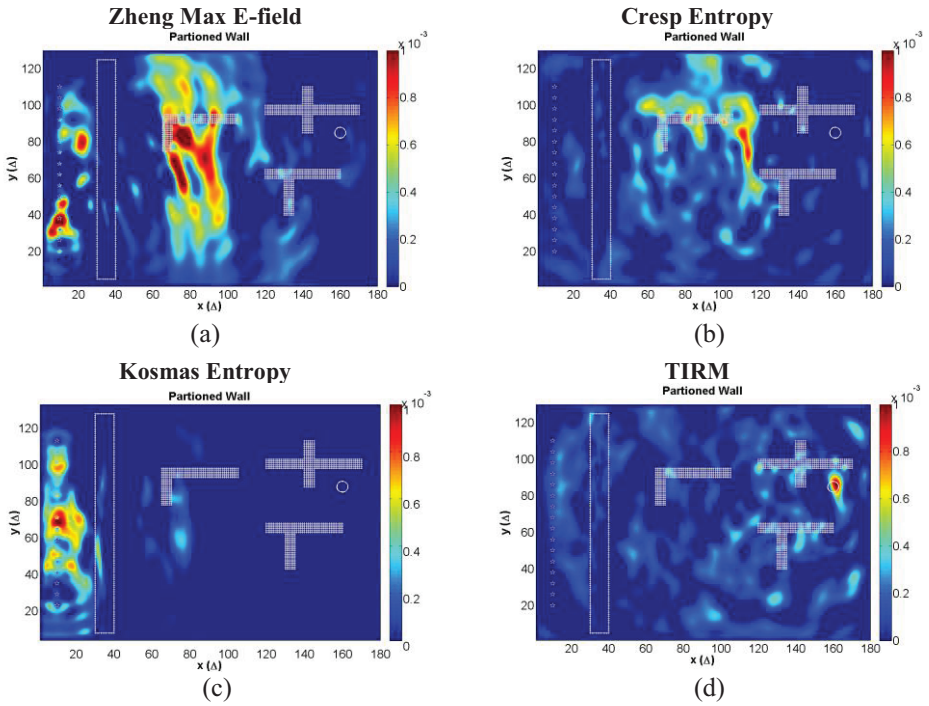

Fig. 9. The images constituted by TR method for target located at far distance: (a) Zheng maximum E-field method, (b) Cresp entropy-based methods Eq. (16), (c) Kosmas entropy-based methods Eq. (17), and (d) TIRM. It is seen only TIRM leads to a true estimation of the target location.

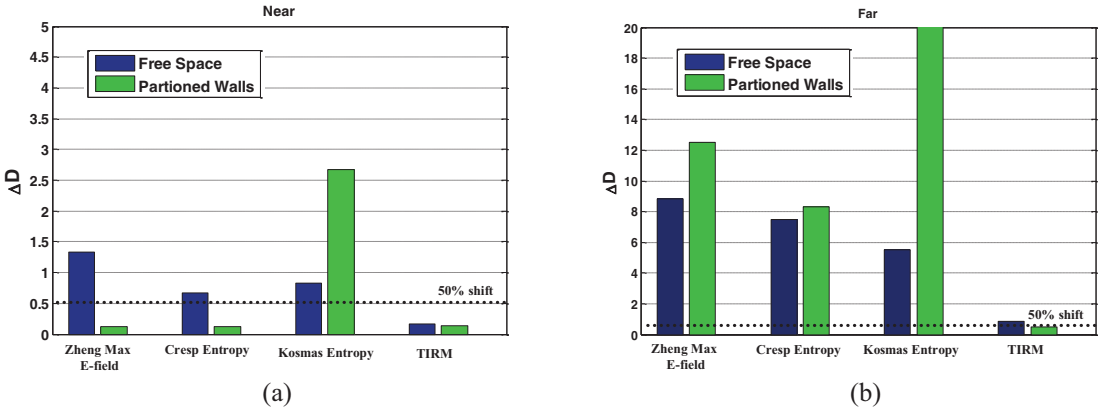

Fig. 10. Difference between estimated and true location of the target for maximum E-field method, entropy-based methods Eq. (16) and Eq. (17), and TIRM. Both free space and rich scattering environment are investigated for: (a) near distance target, and (b) far distance target.

VI. CONCLUSION

In this paper, TR method was employed to detect and localize a target for through-wall microwave imaging (TWMI) problem in a rich scattering environment. Regarding this, the data were generated numerically using FDTD method for both forward and back propagation steps. In order to find the optimum time frame which represents an image of true target location, maximum E-field method, entropy-based methods, and the proposed Target Initial Reflection Method (TIRM) were introduced. The target was placed in two general locations defined as near and far distance. The results showed when the target is located at near distance the performance of almost all methods improved in rich scattering environment compared to free space. However, for far distance in both free space and rich scattering environment, all methods except TIRM significantly failed to accurately estimate the target location. In general, TIRM prevailed over all other methods without being totally dependent on the target

near/far locations and free space or rich scattering background.

Last but not least, future works may include investigating the performance of TR imaging technique and optimum time frame methods with respect to target scattering mode and frequency contents of the excitation signal. In addition, employing this discussion to be gone through for the media of much heterogeneity including biological and under-the-ground imaging applications are of great interest.

REFERENCES

[1] M. G. Amin and F. Ahmad, *Through-the-Wall Radar Imaging: Theory and Applications*, Villanova Univ., Villanova, PA, Sep. 27, 2012.

[2] R. Zetik, S. Crabbe, J. Krajnak, P. Peyerl, J. Sachs, and R. Thoma, "Detection and localization of person behind obstacles using M-sequence through-the-wall radar," in *Proc. SPIE*, vol. 6201, 2006.

[3] X. Liu, H. Leung, and G. Lampropoulos, "Effect of wall parameters on ultra-wideband synthetic aperture through-the-wall radar imaging," *IEEE Trans. Aerosp. Electron. Syst.*, vol. 48, no. 4, pp. 3435-3449, Oct. 2012.

[4] K. M. Yemelyanov, N. Engheta, A. Hoorfar, and J. A. McVay, "Adaptive polarization contrast techniques for through-wall microwave imaging applications," *IEEE Trans. Geosci. Remote Sens.*, vol. 47, no. 5, pp. 1362-1374, May 2009.

[5] F. Soldovieri, R. Solimene, and G. Prisco, "A multiarray tomographic approach for through-wall imaging," *IEEE Trans. Geosci. Remote Sens*., vol. 46, no. 4, pp. 1192-1199, Apr. 2008.

[6] S. Kidera, T. Sakamoto, and T. Sato, "High-resolution 3-D imaging algorithm with an envelope of modified spheres for UWB through-the-wall radars," *IEEE Trans. Antennas Propag*., vol. 57, no. 11, pp. 3521-3529, Nov. 2009.

[7] A. Ishimaru, S. Jaruwatanadilok, and Y. Kuga, "Time reversal effects in random scattering media on superresolution, shower curtain effects, and backscattering enhancement," *Radio Sci*., vol. 42, 2007.

[8] M. Fink, D. Cassereau, A. Derode, C. Prada, P. Roux, M. Tanter, J. Thomas, and F. Wu, "Time-reversed acoustics," *Rep. Prog. Phys*., vol. 63, pp. 1933-1995, 2000.

[9] G. Micolau, M. Saillard, and P. Borderies, "DORT method as applied to ultrawideband signals for detection of buried objects," *IEEE Trans. Geosci. Remote Sens*., vol. 41, no. 8, pp. 1813-1820, Aug. 2003.

[10] H. T. Nguyen, J. B. Andersen, G. F. Pedersen, P. Kyritsi, and P. C. F. Eggers, "Time reversal in wireless communications: a measurement-based investigation," *IEEE Trans. Wireless Commun*., vol. 5, no. 8, pp. 2242-2252, Aug. 2006.

[11] P. Kosmas and C. M. Rappaport, "Time reversal with the FDTD method for microwave breast cancer detection," *IEEE Trans. Microw. Theory Techn*., vol. 53, no. 7, pp. 2317-2323, Jul. 2005.

[12] P. Kosmas and C. M. Rappaport, "FDTD-based time reversal for microwave breast cancer detection: localization in three dimensions," *IEEE Trans. Microw. Theory Techn.*, vol. 54, no. 4, pp. 1921-1927, Apr. 2006.

[13] Y. Chen, E. Gunawan, K. S. Loon, S. Wang, C. B. Soh, and T. C. Putti, "Time-reversal ultrawideband breast imaging: pulse design criteria considering multiple tumors with unknown tissue properties," *IEEE Trans. Antennas Propag*., vol. 56, no. 9, pp. 3073-3077, Sep. 2008.

[14] W. Zheng, Z. Zhao, and Z. Nie, "Application of TRM in the UWB through wall radar," *PIER*, vol. 87, pp. 279-296, 2008.

[15] A. Cresp, I. Aliferis, M. J. Yedlin, Ch. Pichot, and J. Y. Dauvignac, "Investigation of time-reversal processing for surface-penetrating radar detection in a multiple-target configuration," in *Proc. 5th European Radar Conference*, Amsterdam, The Netherland, Oct. 2008.

[16] L. Li, W. Zhang, and F. Li, "A novel autofocusing approach for real-time through-wall imaging under unknown wall characteristics," *IEEE Trans. Geosci. Remote Sens.*, vol. 48, no. 1, pp. 423-431, Jan. 2010.

[17] W. Zhang, A. Hoorfar, and L. Li, "Through-the-wall target localization with time reversal MUSIC method," *PIER*, vol. 106, pp. 75-89, 2010.

[18] A. Taflove and S. C. Hagness, *Computational Electrodynamics: The Finite-Difference Time-Domain Method*, 3rd ed., Boston, MA: Artech House, 2005.

[19] J. P. Stang, "A 3D active microwave imaging system for breast cancer screening," *Ph.D. Dissertation*, Dept. of Elec. Eng., Duke Univ., Durham, NC, 2008.

[20] T. Chan, S. Jaruwatanadilok, Y. Kuga, and A. Ishimaru, "Numerical study of the time-reversal effects on super-resolution in random scattering media and comparison with an analytical model," *Waves in Random and Complex Media*, vol. 18, no. 4, pp. 627-639, Nov. 2008.

[21] D. Liu, S. Vasudevan, J. Krolik, G. Bal, and L. Carin, "Electromagnetic time-reversal source localization in changing media: experiment and analysis," *IEEE Trans. Antennas Propag*., vol. 55, no. 2, pp. 344-354, Feb. 2007.

[22] M. Yavuz and F. L. Teixeira, "Full time-domain DORT for ultrawideband electromagnetic fields in dispersive, random inhomogeneous media," *IEEE*

Trans. Antennas Propag., vol. 54, no. 8, pp. 2305-2315, Aug. 2006.

[23] A. J. Devaney, "Time reversal imaging of obscured targets from multistatic data," *IEEE Trans. Antennas Propag*., vol. 53, no. 5, pp. 1600-1610, May 2005.

[24] J. F. Moura and Y. Jin, "Time reversal imaging by adaptive interference canceling," *IEEE Trans. Signal Process.*, vol. 56, no. 1, pp. 233-247, Jan. 2006.

[25] P. Kosmas and C. M. Rappaport, "A matched-filter FDTD-based time reversal approach for microwave breast cancer detection," *IEEE Trans. Antennas Propag*., vol. 54, no. 4, pp. 1257-1264, Apr. 2006.

[26] N. Maaref, P. Millot, X. Ferrieres, C.Pichot, and O. Picon, "Electromagnetic imaging method based on time reversal processing applied to through-the-wall target localization," *PIER*, vol. 1, pp. 59-67, 2008.

[27] D. Liu, J. Krolik, and L. Carin, "Electromagnetic target detection in uncertain media: time-reversal and minimum-variance algorithms," *IEEE Trans. Geosci. Remote Sens.*, vol. 45, no. 4, pp. 934-944, Apr. 2007.

[28] I. Scott, "Developments in time-reversal of electromagnetic fields using the transmission-line modeling method," *Ph.D. Dissertation*, School of Elec. and Electron. Eng., Univ. of Nottingham, Nottingham, UK, 2009.

[29] D. Liu, G. Kang, L. Li, Y. Chen, S. Vasudevan, W. Joines, Q. H. Liu, J. Krolik, and L. Carin, "Electromagnetic time-reversal imaging of a target in a cluttered environment," *IEEE Trans. Antennas Propag*., vol. 53, no. 9, pp. 3058-3066, Sep. 2005.

[30] G. Montaldo, P. Roux, A. Derode, C. Negreira, and M. Fink, "Ultrasonic shock wave generator using 1-bit time-reversal in a dispersive medium: application to lithotripsy," *Appl. Phys. Lett*., vol. 80, pp. 897-899, 2002.

[31] E. Marengo and F. K. Gruber, "Single-snapshot signal subspace methods for active target location: part II: born-approximable case," *Proc. 2nd IASTED Int. Conf. on Antennas, Radar, and Wave Propag.*, Banff, Alberta, Canada, Jul. 19-21, 2005.

[32] A. Devaney, E. Marengo, and F. Gruber, "Time-reversal-based imaging and inverse scattering of multiply scattering point targets," *J. Acoust. Soc. Amer*., vol. 118, pp. 3129-3138, 2005.

[33] C. Thajudeen, A. Hoorfar, and F. Ahmad, "Measured complex permittivity of walls with different hydration levels and the effect on power estimation of TWRI target returns," *PIER*, vol. 30, pp. 177-199, 2011.

[34] M. Yavuz and F. L. Teixeira, "A numerical study of time-reversed UWB electromagnetic waves in continuous random media," *IEEE Antennas Wireless Propag. Lett.*, vol. 4, pp. 43-46, 2005.

[35] M. Yavuz and F. L. Teixeira, "Frequency dispersion compensation in time reversal techniques for UWB electromagnetic waves," *IEEE Geosci. Remote Sens. Lett.*, vol. 2, no. 2, pp. 233-237, Apr. 2005.

[36] J. D. Taylor, *Ultrawideband Radar: Applications and Design*, CRC Press, 2012.

[37] A. B. Gorji, "Scattering of complex media by using numerical methods in electromagnetics," *M.Sc. Thesis*, Dept. of Elec. Eng., Babol Noshirvani Univ. of Tech., Babol, Iran, 2013.

[38] A. B. Gorji and B. Zakeri, "An improved time-reversal-based target localization for through-wall microwave imaging," *Journal of Electrical and Computer Engineering Innovations (JECEI)*, vol. 1, no. 2, pp. 89-97, 2013.

Amin B. Gorji was born in Cardiff, UK, in 1989. He received the B.Sc. and M.Sc. degrees in Electrical Engineering from Babol Noshirvani University of Technology, Babol, Iran, in 2011 and 2013, respectively. Since 2014, he has been pursuing his Ph.D. in the Department of Electrical and Computer Engineering, Iowa State University, US.

In 2010 to 2014, he has been an Assistant and Researcher with the Antenna and Microwave Laboratory, Babol Noshirvani University of Technology, and starting from 2014 he joined the Center for Non-Destructive Evaluation (CNDE) and Electromagnetic Materials Design and Characterization (EMDC) group of Iowa State University.

His scientific fields of interest include microwave imaging based on time-reversal techniques, Ground-Penetrating Radar (GPR) imaging methods, and microwave non-destructive evaluations.

Bijan Zakeri was born in Babol, Iran, in 1974. He received the M.Sc. and Ph.D. degrees in Electromagnetics Engineering from Amirkabir "Polytechnic" University of Technology, Tehran, Iran, in 1999 and 2007, respectively.

Since 2010, he is an Assistant Professor with Babol Noshirvani University of Technology, Babol, Iran. He is currently the head of Department of Communication and the Director of Antenna and Microwave Laboratory at Babol

Noshirvani University of Technology. He is also a Member of Iranian Association of Information and Communication Technology.

His current research activities are in the fields of computational electromagnetics, microwave imaging, inverse scattering, radar microwave subsystems design, UWB antenna, and Polin-SAR remote sensing.